Tailoring dynamic magnetic characteristics of $Fe_{60}Al_{40}$ films through ion irradiation

N. Tahir,[1] R. Bali,[2] R. Gieniusz,[1] S. Mamica,[3] J. Gollwitzer,[2] T. Schneider,[2] K. Lenz,[2] K. Potzger,[2]
J. Lindner,[2] M. Krawczyk,[3] J. Fassbender,[2,4] and A. Maziewski[1]

[1]*Faculty of Physics, University of Bialystok, ul. Konstantego Ciołkowskiego 1L, Bialystok 15–245, Poland*

[2]*Institut für Ionenstrahlphysik und Materialforschung, Helmholtz-Zentrum Dresden-Rossendorf e.V., 01328 Dresden, Germany*

[3]*Faculty of Physics, Adam Mickiewicz University in Poznan, Umultowska 85, 61–614 Poznan, Poland*

[4]*Institut für Festkörperphysik, Technische Universität Dresden, 01069 Dresden, Germany*

Magnetization dynamics in $Fe_{60}Al_{40}$ thin films possessing depth-varying saturation magnetization (M_S) have been studied experimentally and theoretically. Variation in M_S was achieved by irradiation of 40 nm thick, chemically ordered (B2 phase) $Fe_{60}Al_{40}$ films with Ne^+ ions with energies between 0–30 keV. The initial B2 phase is paramagnetic, and as the penetrating ions cause chemical disordering, the ion-affected region transforms to the ferromagnetic A2 phase. The effective ferromagnetic thickness and the depth of the A2/B2 phase boundary depend on the ion energy (E); the effective thicknesses are 8.5 and 40 nm, respectively, for $E = 2.5$ and 30 keV. Thermally excited spin waves in films with varying effective ferromagnetic thicknesses were analyzed by employing Brillouin light scattering and vector network analyzer ferromagnetic resonance spectroscopy. The analytical calculations are in good agreement with the experimental values and show that the observed spin-wave modes are directly related to the effective ferromagnetic thickness; films irradiated with $E < 15$ keV only show the Damon-Eshbach mode, whereas for $15 \leqslant E < 20$ keV, an additional lower frequency standing spin-wave mode is observed. In films irradiated with $E \geqslant 20$ keV, the Damon-Eshbach mode is observed to lie between two standing spin-wave modes. Furthermore, the A2/B2 phase boundary can be shown to act as an asymmetric pinning site. Controlling the depth of the phase boundary by varying the ion energy can be a path to manipulate spin-wave propagation in materials displaying the phenomenon of disorder induced ferromagnetism.

PACS number(s): 75.30.Ds, 75.70.Cn, 75.78.−n, 75.50.Bb

I. INTRODUCTION

Ion irradiation can serve as a useful tool to induce ferromagnetism in certain alloys consisting of magnetic and nonmagnetic species by inducing chemical disorder. Such systems can provide a base for studying magnetization dynamics in ion-induced magnetic nanostructures [1–6]. From a technological point of view, ion-induced magnetic nanostructures are promising candidates as potential high density data storage, spintronic, magnonics, and magnetoelectronic applications. An example of such an alloy is $Fe_{60}Al_{40}$, where the chemically ordered B2 phase is known to be paramagnetic and can be transformed to the chemically disordered, ferromagnetic, A2 phase through mechanical deformation [1], nanoindentation [7], as well as ion irradiation [2–6].

Materials exhibiting the above phenomena of disorder-induced ferromagnetism have yet to be investigated for their magnetization dynamics properties. Reliable estimates for technologically useful material parameter such as the exchange stiffness (A) are missing.

In the present paper, we have studied the magnetization dynamics of $Fe_{60}Al_{40}$ 40 nm thin films wherein chemical disorder has been systematically induced using ions by vector network analyzer ferromagnetic resonance (VNA-FMR) and Brillouin light scattering (BLS) spectroscopy along with analytical calculations. The saturation magnetization was varied by Ne^+ ion irradiation of initially B2- $Fe_{60}Al_{40}$ films, with ion fluence of 6×10^{14} ions cm^{-2} having energies 0 to 30 keV. The increase in the ion energy leads to an increase in the penetration depth, causing the formation of the A2 phase inside the deeper regions of the film. This implies that the effective thickness of the ferromagnetic phase increases with ion energy.

Furthermore, the A2/B2 phase boundary is gradually pushed deeper into the film and finally expelled when the film is fully penetrated by the ions. The ability to adjust the depth position of the A2/B2 phase boundary helps to investigate the possible pinning effects at this interface. Pinning of spin-wave (SW) modes was considered in the analytical calculations, and a good agreement with the experimental observations shows that adjusting the ion energy can be used as a lever to manipulate the behavior of SWs in these materials.

II. EXPERIMENT

$Fe_{60}Al_{40}$ films of 40 nm thickness were prepared using magnetron sputtering on SiO$_2$(150 nm)/Si(001) substrates. The films were annealed in vacuum at 773 K for 60 minutes to achieve the chemically ordered B2 phase, confirmed with x-ray diffraction. The annealed films are weakly ferromagnetic with saturation magnetization of $M_S = 20$ kAm^{-1}. The B2-$Fe_{60}Al_{40}$ films were irradiated with Ne^+ ions at a fluence of 6×10^{14} ions cm^{-2} with different ion energies, E, in the range of 0 to 30 keV. The M_S varies by ion-induced disorder ferromagnetism to the values of 780 kAm^{-1} (30 keV), which is a factor of 40 larger than that of annealed films. By varying the ion energy, the A2/B2 phase boundary can be gradually pushed deeper into the film until the full film is homogeneously magnetized [see Fig. 1(a)]. The slope of the transient magnetization at the A2/B2 phase boundary may also vary with the ion energy. More details on the sample preparation can be found in Ref. [4].

The dynamic response of the irradiated films was studied by employing VNA-FMR, which allows for the variation
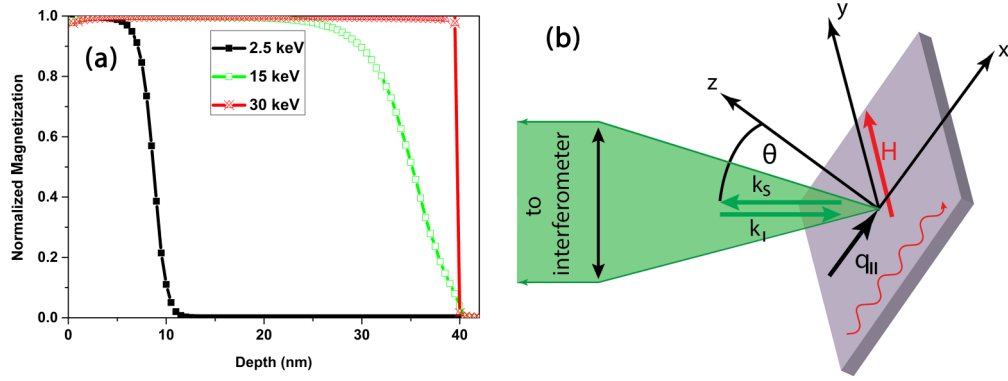
FIG. 1. (Color online) (a) Depth profile of the normalized magnetization for irradiation of the $Fe_{60}Al_{40}$ sample by the Ne^+ ion having energies 2.5 keV, 15 keV, and 30 keV. (b) Scattering geometry of the laser from the sample surface in BLS setup.

of frequency and applied magnetic field [8]. Apart from the situations where nonzero wave vectors are introduced through finite geometry effects (A2/B2 boundary in the present paper), FMR is restricted to dipolar zero-wave–vector SW excitation (uniform mode). An example of nonzero wave vector situation is called standing SWs (SSWs), i.e., exchange-dominated modes with wave vector determined by the layer thickness. BLS spectroscopy with its sub-GHz resolution and high surface sensitivity (∼few nm) for metals is ideally suited for studying A2/B2 phase boundaries. All BLS measurements were performed at room temperature in backscattering geometry [see Fig. 1(b)] using Sandercock (3+3)-pass tandem Fabry-Pérot interferometer to analyze the frequency shift of light from a single-mode solid state laser with $\lambda_{laser} = 532$ nm [9,10]. Inelastically scattered light was sent through a crossed analyzer in order to suppress surface phonons signal. A static magnetic field was applied in the film-plane perpendicular to the transferred wave vector scattering plane, i.e., in the Damon-Eshbach (DE) geometry. The measurements were performed for various magnetic field values and at different angles of incidence of the probing light beam, i.e., the angle between the direction of the incident laser beam and the film normal θ, as shown in Fig. 1(b). The amplitude of the SW transferred in-plane wave vector is related to the angle of incidence θ by the relation $q_{||} = (4\pi/\lambda_{laser})\sin\theta$. By changing θ in the range of 20–60° (this angle restriction is connected with the arrangement of our experimental setup where intensive nonscattered light and limited lens size at low and large θ angle, respectively, are avoided), it is possible to change $q_{||}$ from the range of $(0.8–1.8) \times 10^5$ cm^{-1}.

BLS spectra collected from samples irradiated with ion energies of 2.5 keV, 15 keV, and 30 keV for various applied magnetic fields H and in-plane wave vectors $q_{||}$ are shown in Figs. 2(a)–2(f), respectively. The peaks position in both the Stokes (negative frequencies) and anti-Stokes (positive frequencies) part of the spectrum move towards higher frequencies upon increasing the external magnetic field [Figs. 2(a), 2(c), and 2(d)], revealing their magnetic origin. Depending on the ion irradiation energy (thickness of the modified layer), different modes have been observed. BLS spectra for $\mu_0 H = 0.055$ T and $q_{||} = 0.81 \times 10^5$ cm^{-1} are summarized in Fig. 3.

To better understand the origin of the observed modes and their ion-energy-dependent occurrences, we performed measurements with VNA-FMR to observe the dependence of the field position of the resonance peak on the excitation frequency (Fig. 4). As seen in Fig. 4(a), a single SW frequency mode is observed for the 2.5 keV case, consistent with the BLS spectra of Figs. 2(a) and 2(b). The observed increase in the frequency of this particular mode with increasing ion energy (Fig. 3) can be ascribed to the variation in saturation magnetization M_S with an increase in ion energy observed up to ∼5 keV, i.e., to the thickness of the transient region between A2 and B2 phases. BLS measurements showed that this SW frequency mode has pronounced dispersion with the in-plane wave vector $q_{||}$, and it can be assumed as a magnetostatic surface wave, which propagates in the film plane (also known as the DE mode) [see Figs. 2(b), 2(d), and 2(e)].

In contrast to the case of 2.5 keV Ne^+ irradiation, the $Fe_{60}Al_{40}$ film irradiated with 15 keV Ne^+ showed two SW modes [Fig. 2(c) (BLS) and Fig. 4(b) (VNA-FMR)] with separation of ∼3 GHz at $q_{||} = 0$. Our theoretical analysis will show that in the 15 keV case, [Fig. 2(d)], the higher frequency mode showing a dispersion in dependence on $q_{||}$ can be ascribed to DE mode. The lower frequency mode showed negligible dispersion with $q_{||}$, and we can assume it to be an SSW mode. Furthermore, the sample irradiated with ion energy of 30 keV showed three SW frequencies modes in BLS [Fig. 2(e)], while a single mode was observed in VNA-FMR [see Fig. 4(c)]. Here, the theoretical analysis will show that the low and high frequency modes are the SSW as they are dispersionless, while the middle SW frequency mode shows strong dispersion characteristics on $q_{||}$, confirming it as DE mode.

III. ANALYTICAL RESULTS AND DISCUSSION

In order to understand the origin of experimentally observed SW modes, the experimental data have been fitted by employing two basic formulas: for the DE-modes (i.e., surface magnetostatic SWs propagating perpendicularly to the external magnetic field) and for the exchange SSW-modes. Taking into account the influence of both dipolar and exchange interactions, DE-mode frequency in the system under
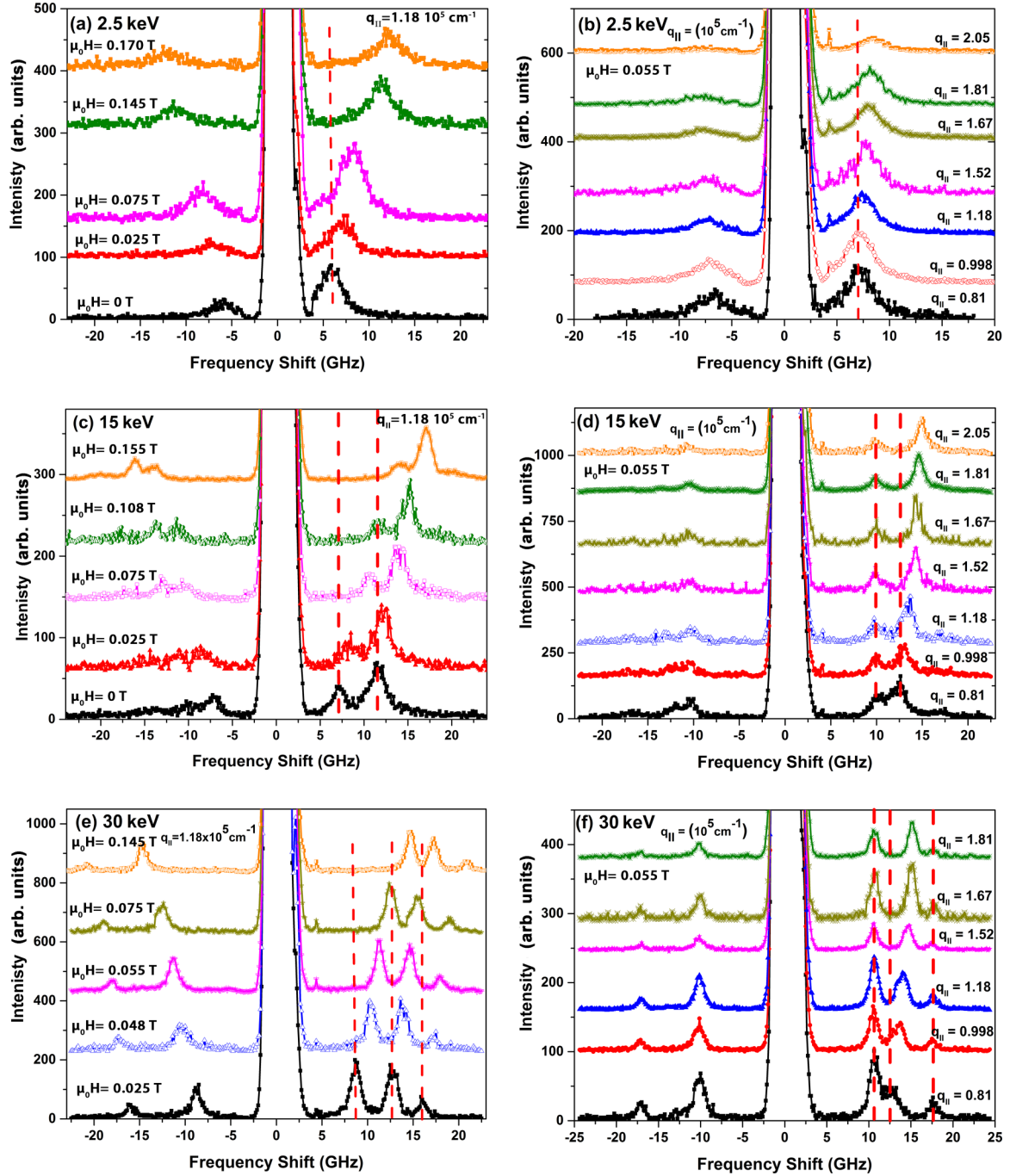
FIG. 2. (Color online) BLS spectra at different applied magnetic field values at a transferred wave vector of 1.18×10^5 cm^{-1}: (a) 2.5 keV, (c) 15 keV, and (e) 30 keV. Dispersion characteristics at a different angle of incidence θ, i.e., different transferred wave vector $q_\parallel$ at an external magnetic field of 0.055 T: (b) 2.5 keV, (d) 15 keV, and (f) 30 keV.

consideration is given as [11]

$$f_{DE} = \frac{\gamma \mu_0}{2\pi} \sqrt{(H + \lambda q_\parallel^2)(H + \lambda q_\parallel^2 + M_S) + \frac{1}{4} M_S[1 - \exp(-2q_\parallel d)]}. \tag{1}$$

Here μ_0 is magnetic permeability, γ is the gyromagnetic ratio (we assume the value of 176.67 GHz/T), d is the thickness of the ferromagnetic film, and $\lambda = 2A/\mu_0 M_S$ with A being the exchange constant. For SSW, we have used the

formula for the purely exchange SWs [11],

$$f_{SSW} = \frac{\gamma \mu_0}{2\pi} \sqrt{(H + \lambda(q_\parallel^2 + q_\perp^2))(H + \lambda(q_\parallel^2 + q_\perp^2) + M_S)}, \tag{2}$$
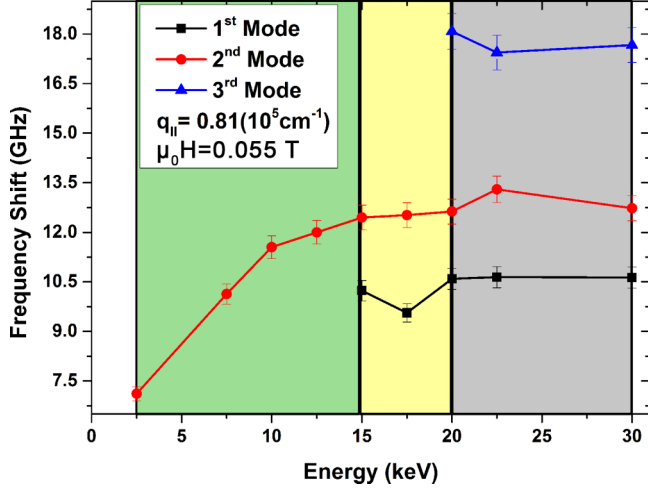
FIG. 3. (Color online) Dependence of observed SW modes on energies of irradiated ions. The data are collected at $\mu_0 H = 0.0550$ T and $q_{||} = 0.81 \times 10^5$ cm^{-1}.

where $q_\perp$ is the wavenumber of the SW across the film thickness. Other parameters are the same as for the DE mode.

Wavenumber $q_\perp$ describes allowed successive standing waves across the film thickness. Its value takes into account the thickness of the A2 phase and pinning of the magnetization dynamics on the film surfaces. The pinning of the SW dynamics at the surface of the ferromagnetic film can have different origin [12–17]. Beside other sources, it can result also from variation of the magnetization or exchange interactions at the outermost area of the ferromagnetic film [18–20]. A continuously vanishing magnetization at the border between phases A2 and B2 [Fig. 1(a)] is only a small part of the whole film. However, this (and the probable associated

change of the exchange constant) can influence SW spectra. Thus, it is reasonable that the border between magnetized and paramagnetic part of the Fe$_{60}$Al$_{40}$ film formed by ion irradiation effectively modifies boundary conditions of the SSW formation and allowed values of $q_\perp$. We will look for $q_\perp$ in the form $q_\perp = (n - \eta)\pi/d$, where n is a mode number and η describes the change of the wavenumber due to pinning and takes values from 0 to 1. We use the standard form of the boundary conditions for the dynamical components of the magnetization vector **m**, to derive η:

$$\left[\frac{\partial \mathbf{m}}{\partial z} + p_{0(d)}\mathbf{m} \right]_{z=0(d)} = 0, \tag{3}$$

where p_0 and p_d are pinning parameters on two boundaries of the film, the free surface, and at the border between A2 and B2 phases, respectively. The derivative is calculated along normal to the film plane (along the z axis).

The relationship between wavenumber $q_\perp$ and pinning parameters for the SSW modes is obtained from solvability condition of Eq. (3) by assuming harmonic solutions for **m** [15,21],

$$\tan\left[q_\perp d \right] = \frac{q_\perp (p_0 + p_d)}{2q_\perp^2 - p_0 p_d}.$$

Assuming natural pinning on the free surface ($p_0 = 0$), one can obtain the following formula for the pinning parameter at the border between A2 and B2 phase in its dependence on η:

$$p_d = \frac{2\pi}{d}(n - \eta)\tan\left[\pi(n - \eta) \right]. \tag{4}$$

We note that in the model considered here, the thickness of the A2 phase d is an ambiguous value, along with the p_d value, because, by inspection of Fig. 1(a), it is clear that d
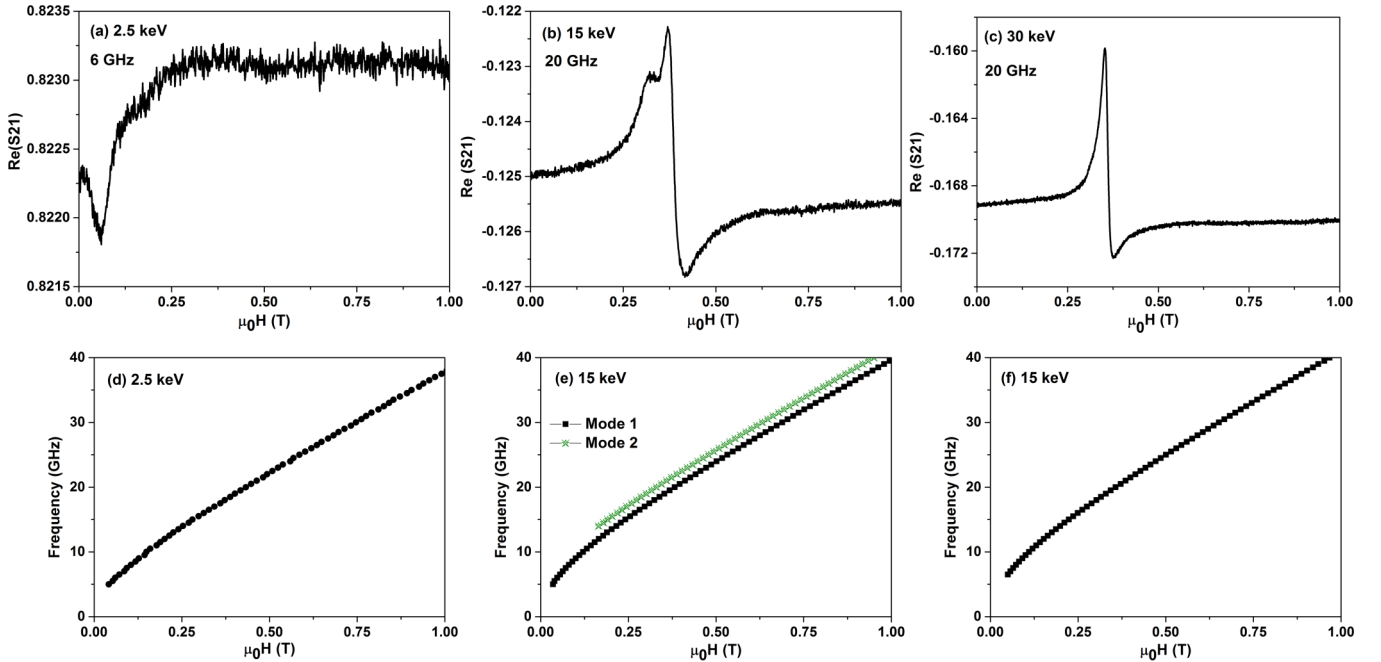

FIG. 4. (Color online) The raw VNA-FMR spectra (inset shows the resonance frequency) for a sample irradiated with energies of 2.5, 15, and 30 keV in (a)–(c), respectively. The measured frequency of spin waves in dependence on the applied magnetic field for sample 2.5, 15, and 30 keV in (d)–(f), respectively.
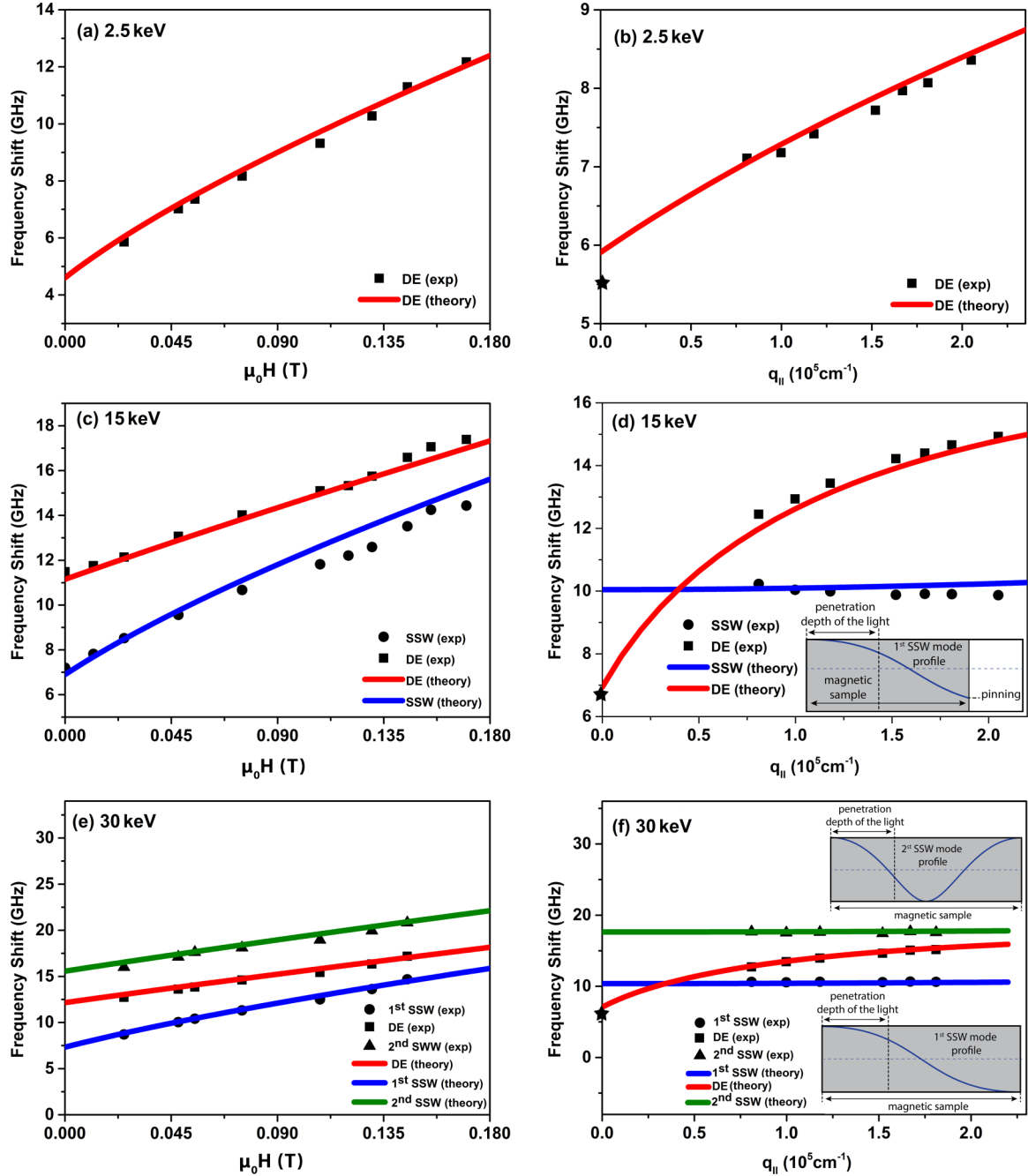
FIG. 5. (Color online) Dependence of the spin-wave frequency on the applied magnetic field at fixed $q_{||} = 0.81 \times 10^5$ cm^{-1} (a), (c), and (e) and transferred wave vector $q_{||}$ at fixed external field $\mu_0 H = 0.055$ T (b), (d), and (f) for samples irradiated with ion energies 2.5 keV (a) and (b), 15 keV (c) and (d), and 30 keV (e) and (f). Solid lines show theory, and solid points show experimental results from measurements by BLS (squares, circles, and triangles) and VNA-FMR (stars). In the insets of (d) and (f), the sketches of the SSW profiles visible in BLS are shown, with the dashed vertical line marking penetration depth of the light in BLS measurements.

can be chosen arbitrarily from the value where magnetization starts to decrease up to the value where it drops to 0. For further consideration, we chose the value d, where M_S takes a value equal to a half of the maximal magnetization saturation; in accordance with Fig. 1(a), these are 40, 35, and 8.5 nm for ion energies of 30 keV, 15 keV, and 2.5 keV, respectively. The most important parameter to interpret is the sign of p_d which suggests the pinning or unpinning of the magnetization at the surface of the film. The estimation of η is free from this ambiguity.

To take into account magnetization pinning at the interface between A2 and B2 phase in Eq. (1), we use an approximate approach by introducing an effective magnetization instead of M_S [22]:

$$M_S \rightarrow M_{S,\mathrm{eff}} \equiv M_S - \frac{2(K_{S1} + K_{S2})}{\mu_0 M_S d}, \qquad (5)$$

where K_{S1} and K_{S2} are surface anisotropy constants at the free surface and the border between A2 and B2 phases, respectively.

TABLE I. Fitting parameters for BLS spectra: thickness of the A2 phase, magnetization saturation, exchange constant, and pinning at A2/B2 interface.

Ion energy (keV)	Magnetic film thickness (nm)	M_S (kA m^{-1})	A (10^{-11} J/m)	Pinning at the A2/B2 interface
2.5	8.5	705	0.41	Yes
15	35	880	0.41	Yes
30	40	880	0.41	No

In accordance with the discussion regarding SSW, we also here assume $K_{S1} = 0$, then Eq. (5) reads

$$M_{S,\text{eff}} \equiv M_S - \frac{2K_{S2}}{\mu_0 M_S d}, \tag{6}$$

where K_{S2} is proportional to the pinning parameter p_d: $K_{S2} = A p_d$ [21].

To estimate effect of the pinning, we fit theoretical curves obtained from Eqs. (1) and (2) to the experimental data obtained from BLS and collected in Fig. 5. The DE mode is strongly dependent on M_S and only slightly on A; thus, we estimated M_S from the fitting of the Eq. (1) to the experimental data. The SSW modes are very sensitive to A and also to the pinning ($q_\perp$), thus Eq. (2) is used to estimate exchange constant. We assume natural pinning on both surfaces ($\eta = 0$, $p_d = 0$, and $K_S = 0$) in the case of 30 keV because the entire thickness of the layer ($d = 40$ nm) is ferromagnetic and mostly homogeneous, with both surfaces sharp. So, for this case, we can find M_S from the fitting of Eq. (1) to the DE mode and A from the fitting of Eq. (2) to the two SSW modes found experimentally [Figs. 5(e) and 5(f)]. The value of 0.880×10^6 A/m and 0.41×10^{-11} J/m is found for M_S and A, respectively, and used throughout the paper. Obtained values of M_S and A are collected also in Table I. Then, we use these values of M_S and A to the sample irradiated with 15 keV. The fitting of Eq. (2) to the BLS results [Figs. 5(c) and 5(d)] required $\eta = 0.3$. From Eq. (4) we get $p_d \approx 0.17$ nm^{-1}, which is comparable with values obtained for FePt thin films [15]. The positive sign of η indicates for so called unpinning, which means the freedom of the spins at the A2/B2 phase boundary are larger than natural [12]. Similar results are presented in Ref. [19], where unpinning was found to be the result of decreasing magnetization, just as in our case. According to the theory of the surface SW [12], the positive [according to the boundary condition Eq. (3)] pinning parameter promotes the surface SWs of the exchange origin (different from the DE mode). They can, however, appear in the measured spectra only when the magnetization saturation is out of plane or at an angle smaller than some critical angle with respect to the normal [23], which is out of the scope of this paper. In the case of 15 keV irradiation, the effective magnetization of the sample, as estimated from Eq. (5), is only slightly lower than M_S, i.e., $M_{\text{eff}} = 0.838 \times 10^6$ A/m. Thus, the influence of the pinning on the DE mode in this case is insignificant. Also for this sample, a good agreement with the experimental data is found for the frequency of the DE mode in dependence on magnitude of the magnetic field as well as on wave vector, as shown in Figs. 5(c) and 5(d), respectively.

For the sample irradiated with the ion energy of 2.5 keV, there is only the DE mode observed in BLS and FMR, thus we need only M_S to fit the experimental data (the SSW are not considered due to its high frequency exceeding the considered range). In this case, the saturation magnetization is expected to be reduced (see Ref. [4]) as compared to its bulk value. In accordance with this, the obtained value from the fitting to Eq. (1) is reduced, as compared to the previous samples taking into account the same pinning as in the previous sample ($p_d \approx 0.17$ nm^{-1} and $M_{\text{eff}} = 0.595 \times 10^6$ A/m).

The light has limiting depth of penetration into the metallic FeAl. If we assume that most of the signal is typically obtained from the top $\sim$10 nm of the film, then, as shown in Fig. 1(b), the signal in the BLS spectrometer under normal incidence is collected from the 1/4 of thickness of the sample 30 keV. In the 15 keV sample, it is collected from 1/3 of the ferromagnetic film thickness and for 2.5 keV from the whole sample. In FMR, the dynamic magnetic radio-frequency field penetrates whole samples, thus the FMR intensity in the homogeneous thin film is proportional to the integral from SW amplitude across the total A2 phase thickness. Samples irradiated with an ion energy of 2.5 keV showed in measurements only single SW mode [Figs. 2(a) and 2(b)]. According to Eq. (2), already the first SSW is out of the experimental range of frequencies, independent on the pinning. Thus, we are not able to estimate the pinning parameter from SSW analysis (we assumed the same value of pinning as for the 15 keV sample). This is consistent with FMR [Fig. 4(a)] measurements, where the only single line is observed, which is the DE mode. In samples irradiated with ion energies of 15 keV, due to the gradual decrease of the magnetization (probably associated with the decrease of the exchange constant) at one surface of the ferromagnetic film, we expect the change of the effective pinning of the magnetization dynamics at this border. For asymmetric boundary conditions, the intensity from the SSW resonances is nonzero, especially for the first SSW [Fig. 5(d)]. The separation between the DE mode and the first SSW at $q_\parallel = 0$ is found to be 3.1 GHz in the 0.055 T magnetic field, which is close to the experimental value [see FMR results in Fig. 4(b)]. At 30 keV, the irradiated ions have enough energy to penetrate the entire sample (i.e., the entire thickness of the sample is ferromagnetic). Because of the limited penetration depth of the BLS, the two lowest SSW modes [Figs. 5(e) and 5(f)] are observed, while the third one is not. In FMR measurements, however, the magnetization dynamics are symmetric on both surfaces (the free magnetization); thus, the FMR intensity from all SSW modes is 0, and the only observed mode is the DE mode Fig. 4(c).

IV. CONCLUSIONS

Magnetization dynamics of disorder induced ferromagnetic Fe$_{60}$Al$_{40}$ thin films have been studied by BLS and VNA-FMR spectroscopy. Depending on energies of the irradiated ions, DE and SSW modes have been identified. For $E < 15$ keV, only the DE mode is detected; for $15 \leqslant E < 20$ keV, a lower frequency SSW is induced; and for $E \geqslant 20$ keV, the DE mode is observed to lie in between two SSW modes. The transient magnetization at the A2/B2 interface acts as the

asymmetric SW pinning site. Ion irradiation of $Fe_{60}Al_{40}$ can therefore provide a way to tune magnetization dynamics, such as by inducing SW pinning at selected film depths. Materials where properties such as the saturation magnetization and SW pinning can be modulated are of huge relevance in the field of magnonics, which seeks to exploit SWs for device applications.

[1] A. Hernando, X. Amils, J. Nogues, S. Surinach, M. D. Baro, and M. R. Ibarra, Phys. Rev. B **58**, R11864 (1998).

[2] J. Fassbender, M. O. Liedke, T. Strache, W. Möller, E. Menéndez, J. Sort, K. V. Rao, S. C. Deevi, and J. Nogués, Phys. Rev. B **77**, 174430 (2008).

[3] E. Menendez, M. O. Liedke, J. Fassbender, T. Gemming, A. Weber, L. J. Heyderman, K. V. Rao, S. C. Deevi, S. Surinach, M. D. Baro, J. Sort, and J. Nogues, Small **5**, 229 (2009).

[4] R. Bali, S. Wintz, F. Meutzner, R. Hübner, R. Boucher, A. A. Ünal, S. Valencia, A. Neudert, K. Potzger, J. Bauch, F. Kronast, S. Facsko, J. Lindner, and J. Fassbender, Nano Lett. **14**, 435 (2014).

[5] N. Tahir, R. Gieniusz, A. Maziewski, R. Bali, M. P. Kostylev, S. Wintz, H. Schultheiss, S. Facsko, K. Potzger, J. Lindner, and J. Fassbender, IEEE Trans. Magn. **50**, 610134 (2014).

[6] N. Tahir, R. Gieniusz, A. Maziewski, R. Bali, K. Potzger, J. Lindner, and J. Fassbender, Opt. Express **23**, 16575 (2015).

[7] J. Sort, A. Concustell, E. Menéndez, S. Suriñach, K. V. Rao, S.C. Deevi, M. D. Baró, and J. Nogués, Adv. Mater **18**, 1717 (2006).

[8] C. Bilzer, T. Devolder, P. Crozat, C. Chappert, S. Cardoso, and P. P. Freitas, J. Appl. Phys. **101**, 074505 (2007).

[9] S. O. Demokritov, B. Hillebrands, and A. N. Slavin, Phys. Rep **348**, 441 (2001).

[10] G. Carlotti and G. Gubbioti, Rivista Del Nuovo Cimento **22**, 1 (1999).

[11] D. Stancil and A. Prabhakar, *Spin Waves: Theory and Applications* (Springer, New York, 2009).

[12] H. Puszkarski, Prog. Surf. Sci **9**, 191 (1979).

[13] B. Hillebrands, P. Baumgart, and G. Güntherodt, Phys. Rev. B **36**, 2450 (1987).

[14] T. G. Rappoport, P. Redlinski, X. Liu, G. Zaránd, J. K. Furdyna, and B. Jankó, Phys. Rev. B **69**, 125213 (2004).

[15] E. Burgos, E. Sallica Leva, J. Gómez, F. Martínez Tabares, M. Vásquez Mansilla, and A. Butera, Phys. Rev **83**, 174417 (2011).

[16] Pedro M. S. Monteiro and D. S. Schmool, Phys. Rev. B **81**, 214439 (2010).

[17] Y. Zhou, H. J. Jiao, Y. T. Chen, G. E. W. Bauer, and J. Xiao, Phys. Rev. B **88**, 184403 (2013).

[18] P. E. Wigen, C. F. Kool, M. R. Shanabarger, and T. D. Rossing, Phys. Rev. Lett **9**, 206 (1961).

[19] M. Sparks, Phys. Rev. B **1**, 3869 (1970).

[20] A. Maksymowicz, Phys. Rev. B **33**, 6045 (1986).

[21] A. G. Gurevich and G. A. Melkov, *Magnetization Oscillations and Waves* (CRC Press, Boca Raton, 1996).

[22] J. P. Nibarger, R. Lopusnik, Z. Celinski, and T. J. Silva, Appl. Phys. Lett. **83**, 93 (2003).

[23] O. G. Ramer and C. H. Wilts, Phys. Stat. Sol. **73**, 443 (1976).